The Astrophysical Journal Letters, 897:L31 (4pp), 2020 July 10 https://doi.org/10.3847/2041-8213/ab9d7b

Optical Detection of the 1.1 day Variability at the White Dwarf GD 394 with TESS

David J. Wilson[1], J. J. Hermes[2], and Boris T. Gänsicke[3]
[1] McDonald Observatory, University of Texas at Austin, Austin, TX 78712, USA; djwilson394gmail.com
[2] Department of Astronomy, Boston University, 725 Commonwealth Avenue, Boston, MA 02215, USA
[3] Department of Physics, University of Warwick, Coventry CV4 7AL, UK
Received 2020 April 16; revised 2020 June 16; accepted 2020 June 16; published 2020 July 10

Abstract

Recent discoveries have demonstrated that planetary systems routinely survive the post-main-sequence evolution of their host stars, leaving the resulting white dwarf with a rich circumstellar environment. Among the most intriguing of such hosts is the hot white dwarf GD 394, exhibiting a unique 1.150 ± 0.003 day flux variation detected in Extreme Ultraviolet Explorer (EUVE) observations in the mid-1990s. The variation has eluded a satisfactory explanation, but hypotheses include channeled accretion producing a dark spot of metals, occultation by a gas cloud from an evaporating planet, or heating from a flux tube produced by an orbiting iron-cored planetesimal. We present observations obtained with the Transiting Exoplanet Survey Satellite (TESS) of GD 394. The space-based optical photometry demonstrates a $0.12 \pm 0.01\%$ flux variation with a period of 1.146 ± 0.001 days, consistent with the EUVE period and the first re-detection of the flux variation outside of the extreme ultraviolet. We describe the analysis of the TESS light curve and measurement of the optical variation, and discuss the implications of our results for the various physical explanations put forward for the variability of GD 394.

Unified Astronomy Thesaurus concepts: White dwarf stars (1799); Variable stars (1761); Exoplanets (498)

1. Introduction

GD 394 is a hot, metal-polluted white dwarf that has challenged interpretation since its initial identification by Giclas et al. (1967). Indeed, both of the descriptions in the preceding sentence are unquantified: estimates for the effective temperature vary from 33,000 to 41,000 K (Barstow et al. 1996; Lajoie & Bergeron 2007) and the measured metal abundances, accretion rates, and species depend on the wavelength band and ionization levels observed (Wilson et al. 2019). However, the most intriguing aspect of GD 394 is the detection by Christian et al. (1999) and Dupuis et al. (2000) of a sustained 25% modulation of the extreme ultraviolet (EUV; 70–380 Å) flux with a period of 1.15 days in observations made in 1992–1996 with multiple instruments on board the Extreme Ultraviolet Explorer (EUVE) satellite. So far, this large-amplitude EUV modulation is unique among white dwarfs, and was hypothesized to be due to opacity changes induced by a spot of accreting metals moving in to and out of view with the white dwarf rotation.

The metal spot hypothesis made two observable predictions. First, the strength of the metal lines in the white dwarf spectrum should vary in phase with the EUV variation. Second, there should be an anti-phase flux variation at optical wavelengths due to flux redistribution. Follow-up observations by Wilson et al. (2019) ruled out the first of these predictions, finding no change in the strength of strong Si, Fe, and Al absorption lines in eight Hubble Space Telescope (HST) far-ultraviolet (FUV; 1160–1700 Å) spectra sampling the full (putative) white dwarf spin cycle. They also searched SuperWASP photometry for optical variability, ruling out $\gtrsim$1% changes in flux. Instead of a spot model, Wilson et al. (2019) favored a circumstellar explanation such as a gas cloud generated by an evaporating but non-transiting planet, similar to the ice giant detected in an ≈8–10 day orbit of WD J0914+1914 by Gänsicke et al. (2019). Veras & Wolszczan (2019) alternatively suggested that an orbiting, iron-rich planetesimal core could induce a magnetic flux tube connecting it to the white dwarf in GD 394, heating the photosphere at the base of the tube to produce a hot spot.

Here, we present observations of GD 394 obtained using the Transiting Exoplanet Survey Satellite (TESS; Ricker et al. 2014) demonstrating that GD 394 is indeed varying in the optical with a period in agreement with that detected previously in the EUV, but with a much smaller amplitude. Section 2 details our analysis of the TESS light curve. Section 3 discusses the implications of the optical re-detection for the physical explanation of the variation at GD 394.

2. Observations

GD 394 (TIC 259773610, $T = 13.4$ mag) was observed by TESS in Camera 2 for 52 days in Sectors 15 and 16 (2019 August 15–2019 October 6), with three roughly one-day gaps at spacecraft perigee.[4] Data was returned with a two minute cadence as requested in proposals G022077, G022028, and G022017, and processed using the Pre-Search Data Conditioning Pipeline (PDC; Stumpe et al. 2012) to remove common known instrumental trends.

We analyzed the light curves from each sector separately. The light curves were retrieved from MAST[5] and points marked with a quality flag were removed, as were any 5σ outliers above the median flux. The flux was normalized by subtracting a second-order polynomial fit. We generated Lomb–Scargle periodograms using the `Lightkurve` package (Lightkurve Collaboration 2018; Figure 1, top row). A ≈ 1.15 day period is clearly detected in each sector, providing the first confirmation of the EUVE detection beyond the extreme ultraviolet.

The Sector 15 periodogram contained a second peak at ≈0.98 day (orange dashed line in Figure 1). Using the TESS pixel data, we found that this signal originates from a nearby

[4] See TESS Data Release Notes at http://archive.stsci.edu/tess/tess_drn.html.
[5] https://archive.stsci.edu/

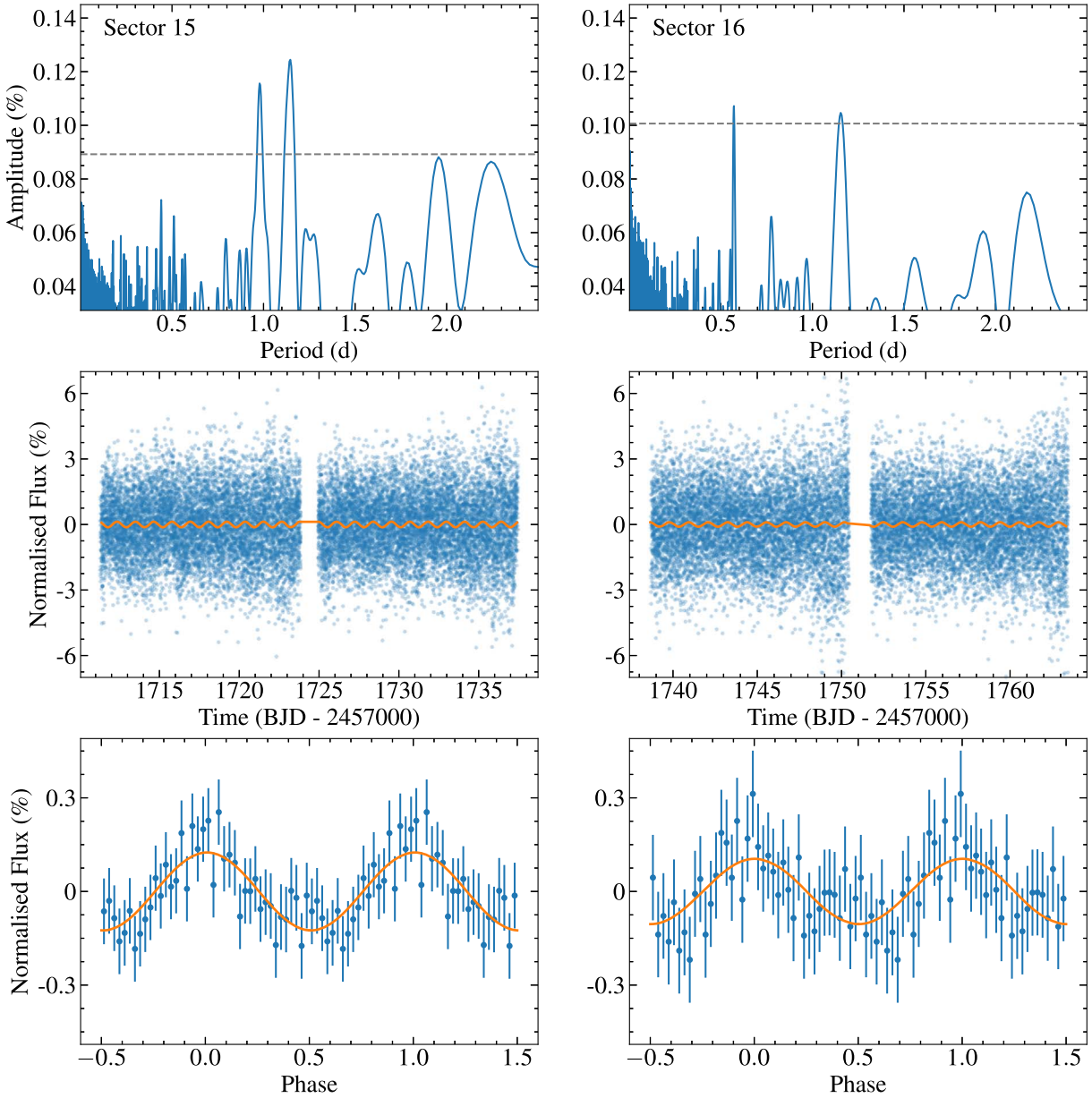

Figure 1. Top row: periodograms of the TESS light curves of GD 394 from Sectors 15 and 16. The gray dashed line shows the 99% false alarm probability (FAP) signal apparent in each sector, as discussed in the text. Significant signals at 1.1459 ± 0.0033 days and 1.1547 ± 0.0051 days are detected in Sector 15 and 16, respectively. The ≈0.98 day signal apparent in Sector 15 is due to contamination from a nearby giant star. The first harmonic ($P/2$) of the 1.15 day signal is detected in Sector 16. Middle row: TESS light curves of GD 394 together with the sine fit used to measure the period and amplitude of the variation. The enhanced scatter at the end of each segment of the light curve is due to increased background earthshine as the spacecraft approaches perigee. Bottom row: light curves folded onto the fitted period and binned to 40 steps. The cycle is repeated for clarity, and the model fit is overplotted in orange.

giant star, TIC 259773551 (TESS magnitude = 12.9). We have therefore ignored this periodicity; it only marginally adds to our systematic uncertainties.

To ascertain the significance of the detected signals we calculated the false alarm probability (FAP) via the method described in Hermes et al. (2017) and Bell et al. (2019). In short, we generated 10,000 synthetic light curves for each sector, using the same time-axis but randomly shuffling the flux values. A periodogram was calculated for each synthetic light curve and the maximum amplitude recorded. We defined our 1% FAP as the power below which the maximum amplitude in 99% of our synthetic light curves fell (gray dashed line in Figure 1). As the signals in each light curve exceed this limit, we conclude that there is a less than one percent probability that our detected signal is due to random chance in each sector, and therefore a <0.01% chance of observing the same, random signal in both sectors. A $P/2$ harmonic of the expected signal is also detected with <1% FAP in Sector 16.

We then fit a sinusoid to each light curve using the peak measured from the periodogram as an initial guess for the period, shown in the middle panel of Figure 1. The bottom panel shows the data folded onto the fitted period, clearly demonstrating the sinusoidal nature of the signal.

The periods and amplitudes for each sector are consistent to within 3σ, so we do not formally detect any amplitude or phase variability between the two sectors. However, the shape of the power spectrum is notably different between the two sectors. In particular, the amplitude of the 1.1547 ± 0.0051 day signal in

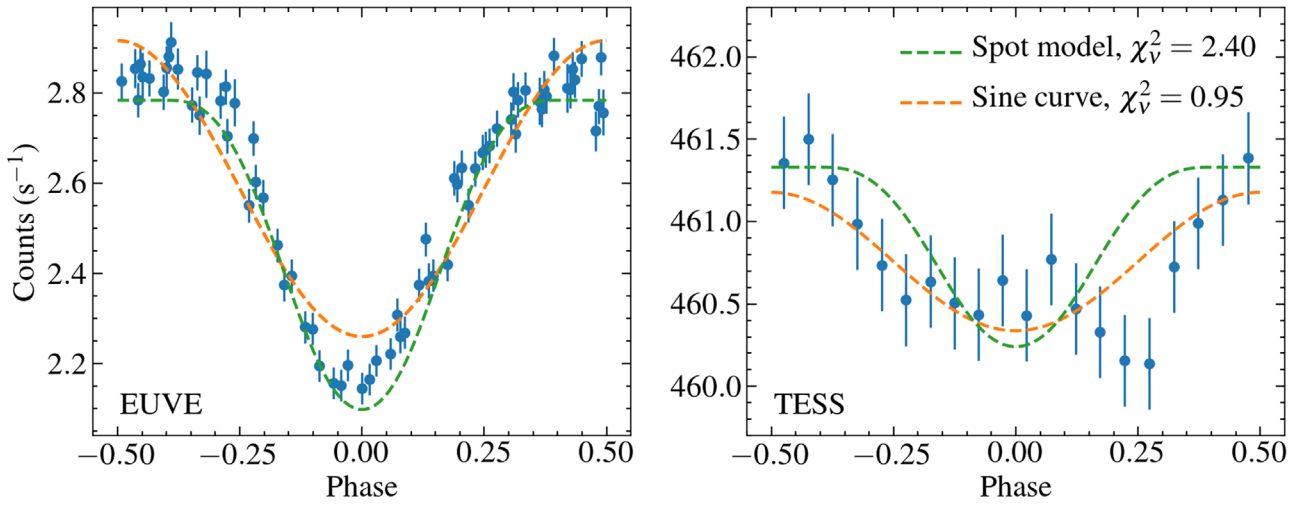

Figure 2. Comparison of the EUVE and TESS signals. Left panel: recreation of Figure 6 of Dupuis et al. (2000) showing the EUVE DS light curve. Right panel: 2-sector TESS light curve folded onto the measured 1.1468 day period and binned to 20 points. In both panels the dashed green and orange lines show model fits to each light curve using the Dupuis et al. (2000) spot model and a sinusoidal, respectively.

Table 1
Measured Periods and Amplitudes for the Variation at GD 394

Sector	Mid-MJD (days)	Period (days)	Amplitude (%)
EUVE	≈50000	1.15 ± 0.003	≈25
15	58724	1.1459 ± 0.0033	0.127 ± 0.016
16	58750	1.1547 ± 0.0051	0.102 ± 0.018
15 + 16	58736	1.1468 ± 0.0014	0.117 ± 0.012
Ephemeris (BJD):	2458737.560 ± 0.018		

Note. EUVE measurements from Dupuis et al. (2000) are given as approximations as observations were obtained at multiple epochs with different instruments.

Sector 16 is weaker than the 1.1459 ± 0.0033 day signal in Sector 15, and the $P/2$ harmonic is clearly detected in Sector 16 but not Sector 15.

We combined the light curves from both sectors and repeated the analysis, finding a period of 1.1466 ± 0.0015 days and an amplitude 0.117 ± 0.012% in the TESS bandpass, centered at a wavelength of roughly 786.5 nm. The ephemeris is defined as the peak of the model fit closest to the mid-point of the TESS observations, $T_{\rm Ephemeris}$ = 2458737.560 ± 0.018 (BJD). Table 1 summarizes the various period and amplitude measurements for GD 394 from TESS and EUVE.

3. Discussion

The P = 1.145 ± 0.006 day periodic variation of GD 394 in the TESS light curve is consistent with the 1.150 ± 0.003 day period measured in the EUVE data by Dupuis et al. (2000), with no strong evidence for period evolution in the roughly 24 yr between the observations. On the other hand, the optical amplitude of 0.117 ± 0.012% is much smaller than the ≈25% variation in the EUV, and below the ≈1% upper limits placed on FUV variation by Wilson et al. (2019).

Figure 2 compares the folded EUVE light curve and best-fit spot model from Dupuis et al. (2000) with the folded TESS light curve. Dupuis et al. (2000) adopted a model where the spot is completely dark, with the ratio of the flux of the spot to the photosphere $kw = 0$. To investigate whether the same spot is causing the TESS variation, we fit a model keeping the geometry of the best-fit EUV model but varying the opacity. We find an ≈1% flux ratio (i.e., $kw \approx 0.99$ in the Dupuis et al. 2000 notation) provides a reasonable match to the folded TESS light curve. However, the sinusoidal model used to measure the period is statistically a better fit to the TESS data despite being a poor model for the EUVE light curve. The poor signal-to-noise ratio of the TESS data dominates the fit, so confidently distinguishing between different models, and confirming whether the optical variation definitely has the same origin as the EUV variation, is not possible.

Optical variation was a prediction of the metal spot model favored by Dupuis et al. (2000) as an explanation for the EUV variation. However, the metal spot model was not supported by the non-detection of changes in FUV metal absorption line strengths by Wilson et al. (2019). It is possible that the spot has a variable opacity, appearing strongly at the time of the 1993–1996 EUVE observations, fading by the time of the 2015 HST observations but returning in time to be observed with 2019 TESS observations (with the period fixed by the white dwarf rotation period). However, this is likely too strong an appeal to coincidence, especially considering that Si absorption line strengths in the 2015 HST spectra were consistent with the strengths of the same lines detected in HST spectra obtained in 1992 by Shipman et al. (1995). Figure 2 shows that a lower opacity version of the spot model fitted to the EUVE data does does not exactly describe the TESS light curve, raising the possibility that the geometry of the spot may have changed. If the TESS mission is extended long enough for GD 394 to be reobserved then tests for changes in the variation amplitude and shape will be possible.

We are left requiring a mechanism that will generate flux variations of 25% in the EUV, 0.117% in the optical, and $\lesssim$1% in the FUV (the upper limit placed by light curves extracted from the time-tagged HST spectroscopy by Wilson et al. 2019). The suggestion by Veras & Wolszczan (2019) that the variation is due to a hot spot at the base of a magnetic flux tube may fit these criteria, as a sufficiently hot spot could provide the required amplitude in the EUV, with the flux quickly dropping away in the Rayleigh Jeans tail to the low levels observed at longer

wavelengths. However, this would require spot temperatures of $\gtrsim 10^5$ K, and thus far no magnetic field has been detected in high-resolution spectroscopy of GD 394 ($B_e \leqslant 12$ kG; Dupuis et al. 2000; Wilson et al. 2019). The generation of a flux tube requires an orbiting metal-rich planetary fragment which may be radio-loud, and thus radio observations might provide an opportunity to test this model.

The various explanations for the flux variations at GD 394, including metal spots, occultation by an outflow from an orbiting planet, or a magnetically induced hot spot, could be tested by searching for phase differences between the two wavebands: out of phase variation would favor a metal spot; in-phase variation would point to a circumstellar cause or a hot spot. In practice, phasing up the EUVE and TESS observations is impossible given cycle-count ambiguities in the decades-long gap between them. Therefore, new contemporaneous EUV and high-precision optical observations are required, although this will be challenging given the currently available observing facilities.

The TESS detection strengthens the connection between GD 394 and WD J1855+4207 suggested by Hallakoun et al. (2018), both stars having high (>30,000 K) effective temperatures, high ionization-level metal absorption lines with strengths well above those predicted by their effective temperatures, and weak, many-hour period optical modulation (Maoz et al. 2015). Proposed future missions such as ESCAPE (France et al. 2019) could search for EUV variation at WD J1855+4207, confirming whether or not it is truly a GD 394 analog.

In conclusion, the TESS observations of GD 394 reveal the same 1.15 day periodicity at optical wavelengths that was initially identified in the EUV more than two decades ago. The very small amplitude of the optical modulation, 0.12%, explains why this signal remained undetected in previous ground-based observations of GD 394. A physical explanation for the modulation now detected in two wavebands remains elusive.

We thank A. Vanderburg for useful advice regarding contamination from nearby stars in TESS, and J. Dupuis for sharing the EUVE light curves. J.J.H. acknowledges support by the National Aeronautics and Space Administration through the TESS Guest Investigator Program (80NSSC19K0378). This Letter includes data collected by the TESS mission. Funding for the TESS mission is provided by the NASA Explorer Program.

Facility: TESS.

Software: Astropy (Astropy Collaboration 2018), Lightkurve (Lightkurve Collaboration 2018).

ORCID iDs

David J. Wilson https://orcid.org/0000-0001-9667-9449
J. J. Hermes https://orcid.org/0000-0001-5941-2286
Boris T. Gänsicke https://orcid.org/0000-0002-2761-3005

References

Astropy Collaboration, Price-Whelan, A. M., Sipőcz, B. M., et al. 2018, AJ, 156, 18
Barstow, M. A., Holberg, J. B., Hubeny, I., et al. 1996, MNRAS, 279, 1120
Bell, K. J., Córsico, A. H., Bischoff-Kim, A., et al. 2019, A&A, 632, A42
Christian, D. J., Craig, N., Cahill, W., Roberts, B., & Malina, R. F. 1999, AJ, 117, 2466
Dupuis, J., Chayer, P., Vennes, S., Christian, D. J., & Kruk, J. W. 2000, ApJ, 537, 977
France, K., Fleming, B. T., Drake, J. J., et al. 2019, Proc. SPIE, 11118, 1111808
Gänsicke, B. T., Schreiber, M. R., Toloza, O., et al. 2019, Natur, 576, 61
Giclas, H. L., Burnham, R., & Thomas, N. G. 1967, LowOB, 7, 49
Hallakoun, N., Maoz, D., Agol, E., et al. 2018, MNRAS, 476, 933
Hermes, J. J., Gänsicke, B. T., Kawaler, S. D., et al. 2017, ApJS, 232, 23
Lajoie, C., & Bergeron, P. 2007, ApJ, 667, 1126
Lightkurve Collaboration, Cardoso, J. V. d. M., Hedges, C., et al. 2018, Lightkurve: Kepler and TESS Time Series Analysis in Python, Version 1.2.0, Astrophysics Source Code Library, ascl:1812.013
Maoz, D., Mazeh, T., & McQuillan, A. 2015, MNRAS, 447, 1749
Ricker, G. R., Winn, J. N., Vanderspek, R., et al. 2014, Proc. SPIE, 9143, 914320
Shipman, H. L., Provencal, J., Roby, S. W., et al. 1995, AJ, 109, 1220
Stumpe, M. C., Smith, J. C., Van Cleve, J. E., et al. 2012, PASP, 124, 985
Veras, D., & Wolszczan, A. 2019, MNRAS, 488, 153
Wilson, D. J., Gänsicke, B. T., Koester, D., et al. 2019, MNRAS, 483, 2941